Published in final edited form as:
Synapse. 2012 May ; 66(5): 418–434. doi:10.1002/syn.21530.

Nicotinic acetylcholine receptors in rat forebrain that bind ^{18}F-nifene: relating PET imaging, autoradiography and behavior

Kasia M. Bieszczad[2,4,*], **Ritu Kant**[1,*], **Cristian C. Constantinescu**[1,*], **Suresh K. Pandey**[1], **Hideki D. Kawai**[2,5], **Raju Metherate**[¶,2,3,4], **Norman M. Weinberger**[2,3,4], and **Jogeshwar Mukherjee**[1]

[1]Preclinical Imaging Center and Department of Psychiatry & Human Behavior, University of California, Irvine, CA

[2]Department of Neurobiology & Behavior, University of California, Irvine, CA

[3]Center for Hearing Research, University of California, Irvine, CA

[4]Center for the Neurobiology of Learning and Memory, University of California, Irvine, CA

[5]Department of Bioinformatics, Faculty of Engineering, Soka University, Hachiouji, Tokyo

Abstract

Nicotinic acetylcholine receptors (nAChRs) in the brain are important for cognitive function; however, their specific role in relevant brain regions remains unclear. In this study we used the novel compound ^{18}F-nifene to examine the distribution of nAChRs in the rat forebrain, and for individual animals related the results to behavioral performance on an auditory-cognitive task. We first show negligible binding of ^{18}F-nifene in mice lacking the β2 nAChR subunit, consistent with previous findings that ^{18}F-nifene binds to α4β2* nAChRs. We then examined the distribution of ^{18}F-nifene in rat using three methods: *in vivo* PET, *ex vivo* PET and autoradiography. Generally, ^{18}F-nifene labeled forebrain regions known to contain nAChRs, and the three methods produced similar relative binding among regions. Importantly, ^{18}F-nifene also labeled some white matter (myelinated axon) tracts, most prominently in the temporal subcortical region that contains the auditory thalamocortical pathway. Finally, we related ^{18}F-nifene binding in several forebrain regions to each animal's performance on an auditory-cued, active avoidance task. The strongest correlations with performance after 14 days training were found for ^{18}F-nifene binding in the temporal subcortical white matter, subiculum and medial frontal cortex (correlation coefficients, $r > 0.8$); there was no correlation with binding in the auditory thalamus or auditory cortex. These findings suggest that individual performance is linked to nicotinic functions in specific brain regions, and further support a role for nAChRs in sensory-cognitive function.

Keywords

nicotine; learning; memory; auditory; thalamocortical; prefrontal

Introduction

Nicotinic regulation of neural processing is important for sensory-cognitive function, as demonstrated in physiological and behavioral studies (Hasselmo and Sarter, 2011; Levin et

[¶]Correspondence: Raju Metherate, Ph.D., Department of Neurobiology and Behavior, University of California, Irvine, 2205 McGaugh Hall, Irvine CA 92697; raju.metherate@uci.edu, phone: 949-824-6141, fax: 949-824-2447.
[*]equal contribution

al., 2006; Perry et al., 2000). Nicotine and other agonists enhance performance on cognitive tests, and conversely, the loss of forebrain nAChRs is associated with cognitive decline. Although studies indicate that nicotinic function is important for cognition, the relationships among nAChR functions, neural systems and behavior are not well understood.

One approach to understanding this relationship is to relate nicotinic function in specific neural circuits to behavior. For example, nicotine-induced enhancement of auditory cortex function correlates well with auditory-cued behavior in rats, i.e., good performers on an active avoidance task exhibit stronger nicotine effects (Liang et al., 2008). Similarly, good performance on a cortex-dependent task is associated with a higher density of nAChRs in hippocampus and neocortex in rabbits (Li et al., 2008). Intriguingly, naturally-occurring mutations that enhance nAChR function are linked to enhanced cognitive performance in humans (Espeseth et al., 2010). While it may seem surprising that normal variation in cognitive function may result from variation in a single neurotransmitter receptor, the success of this approach may reflect the importance of nAChRs for cognition. To examine this issue further, in the present study we assessed the feasibility of relating behavior to nAChR function as determined non-invasively with PET imaging.

In PET studies, radioligands are used to image nAChRs (reviewed by Horti et al., 2010), with the recent introduction of ^{18}F-nifene proving effective for imaging α4β2* nAChRs (asterisk indicates presence of additional subunits) with significantly shorter scan times than existing radioligands (e.g., 40–60 min vs. several hours) (Easwaramoorthy et al., 2007; Hillmer et al., 2011; Kant et al., 2011; Pichika et al., 2006). Results across binding studies are largely consistent with the distribution of α4β2* nAChRs in earlier studies. A notable exception is a PET study demonstrating strong, putative α4β2* nAChR binding in the human temporal subcortical white matter, an unexpected finding since neurotransmitter receptors are not thought to function in myelinated axon pathways (Ding et al., 2004). However, a subsequent physiological study showed that nAChRs regulate axon excitability for myelinated axons in the mouse auditory thalamocortical pathway (Kawai et al., 2007). Thus, nicotinic regulation of thalamocortical axons can enhance sensory-evoked cortical responses, which in turn could enhance cognitive processing of sensory stimuli (Metherate, 2011).

The present study was conceived as a first step towards relating nicotinic function in specific brain regions to behavior. We first determined the distribution of ^{18}F-nifene using *in vivo* PET, *ex vivo* PET and autoradiography in rats, wild-type mice and mice lacking β2 nAChRs, and then correlated nAChR levels in selected brain regions with behavioral performance for a subgroup of rats. Regions of interest selected for correlation of ^{18}F-nifene binding with behavior were selected either for relevance to auditory processing or for known density of nAChRs. The results show that auditory-cognitive performance is correlated positively with ^{18}F-nifene binding in a subset of brain areas including frontal cortex, subiculum, and, exclusively among auditory regions, the temporal subcortical white matter.

Materials and Methods

All animal procedures were performed in accordance with NIH guidelines and approved by the University of California, Irvine IACUC. Rats used for PET studies were first characterized behaviorally, then scanned and the data analyzed with the experimenter blind to behavioral results. For experiments in mice, subjects were either wild type or transgenic mice lacking the β2 nAChR subunit (Picciotto et al., 1995).

General imaging methods

All chemicals and solvents were purchased from Aldrich Chemical and Fisher Scientific. Deonized water was acquired using a Millipore Milli-Q Water Purification System. Gilson high performance liquid chromatography (HPLC) was used for the semipreparative reverse-phase column chromatography. Fluorine-18 fluoride was produced via MC-17 Scanditronix cyclotron using oxygen-18 enriched water. Radioactivity was counted using a Capintec dose calibrator while low level counting was done using a well-counter. An Inveon preclinical dedicated PET (Siemens Medical Solutions, Knoxville, TN) with a transaxial FWHM of 1.46 mm, and axial FWHM of 1.15 mm (Bao et al., 2009; Constantinescu and Mukherjee, 2009) was used for the PET studies. Both *in vivo* and *ex vivo* PET images of rat brains were obtained and analyzed using Acquisition Sinogram Image Processing (ASIPRO) and Pixelwise Modeling Software (PMOD) software. For autoradiography, brain slices were prepared at 10–40 μm thick using a Leica 1850 cryotome. Labeled sections were exposed to phosphor films (Perkin Elmer Multisensitive, Medium MS) and read using the Cyclone Phosphor Imaging System (Packard Instruments). Analysis of autoradiographs was done using Optiquant acquisition and analysis software.

PET experiments

Radiolabeling: Synthesis of ^{18}F-nifene was carried out following reported procedures (Pichika et al., 2006). The automated radiosynthesis of ^{18}F-nifene was carried out in the CPCU (chemistry-processing control unit) box. An Alltech C_{18} column (10 μm, 250 x 10mm^2) was used for reverse-phase HPLC purification and specific activity of ^{18}F-nifene was approximately 2000 Ci/mmol.

Animal handling: In preparation for scanning, rats and mice were housed in individual cages in a climate-controlled room (24°C) with a 12:12-hour light cycle. Subjects had free access to food and water until the day of imaging, and then were fasted in the imaging room, in a dark quiet place, for 4–6 hours prior to experiments. Prior to the scan, animals were placed in an induction chamber and anesthetized with isoflurane at 4% concentration. Animals were maintained under anesthesia throughout the scan with 2% isoflurane delivered via a nose-cone. Body temperature was maintained with a water-circulating heating pad.

***In vivo* imaging:** Rats were injected with 31.5 ± 5.3 MBq of ^{18}F-nifene and scanned for 90 min in the Inveon scanner. List-mode data were histogrammed in 45 time frames (10 x 0.5 min, 15 x 1 min, 10 x 2 min, 10 x 5 min). WT and β2-KO mice were injected with 9.63 ± 0.85 MBq of ^{18}F-nifene and scanned for 30 min, starting 30 min post injection. Random events were subtracted prior to reconstruction. The images were reconstructed using Fourier rebinning and 2-dimensional filtered back-projection (2D FBP) method (Hanning filter and cutoff at Nyquist frequency) with an image matrix of 128x128x159, resulting in a pixel size of 0.77 mm and a slice thickness of 0.796 mm. All dynamic images were corrected for radioactive decay. Attenuation correction was performed using a 10-min transmission scan with a ^{57}Co point source performed prior to tracer injection. Normalization of detector responses was also applied using a cylinder source inversion method.

***Ex vivo* imaging and autoradiography:** Immediately following *in vivo* acquisition, animals were sacrificed by decapitation. The brain was excised, placed in a dish, and frozen on a bed of dry ice. The brain was then imaged for 30 minutes in the PET scanner. The same imaging parameters as for *in vivo* imaging were used. Following *ex vivo* imaging the brains were sectioned at 20 μm. Approximately 40 sections were laid on glass slides, placed on film and left overnight. The following day, film was exposed using a Cyclone Phosphor Imaging System.

Image Analysis: Processing of reconstructed images was performed with PMOD software package (PMOD Technologies). PET images were normalized to the standard space described by the stereotaxic coordinates of Paxinos & Watson (Paxinos and Watson, 1986) via co-registration to an MRI rat template (Schweinhardt et al., 2003). The size of the template image was 80 x 63 x 108 voxels with a voxel size of 2 mm. The template includes a scale factor of 10 in order to roughly match the size of the human brain and facilitate analysis with SPM software. Bregma was set as the origin of coordinates system. The spatial extent of the template volume (bounding box) was from −80 to 80 mm in X direction (left to right of the midline, through the sagital planes), −120 to 6 mm in the Y direction (ventral to dorsal, through the horizontal planes) and from −156 to 60 mm in the Z direction (posterior to anterior, through the coronal planes). 3D volumes of interest (VOIs) were drawn on the MR template for thalamus (TH), striatum (STR), frontal cortex (FC), subiculum (SUB), temporal subcortical white matter (TSW), and cerebellum (CB). The placing of the VOIs was guided by examination of the Paxinos & Watson rat atlas (4th edition). The VOI over TH (11.1 mm^3) was a prolate ellipsoid with the center at (x,y,z) = (0.0, −60.4, 32.0) mm, a long axis of 53 mm in X direction, and a short axis of 20 mm. VOI on STR consisted of a series of elliptical 2D regions placed bilaterally and symmetrically with respect to the midline on multiple horizontal planes with the center of mass at (+\−14, −38, −70) mm (right\left STR, 5 mm^3). The VOIs on FC consisted of irregular 2D regions placed on multiple coronal planes, with the centers of mass at (+\−13.4, −42.5, 34) mm (right\left FC, 3.2 mm^3), (+\−47, −49, −30.9) mm (right\left TSW, 0.1 mm^3), (+\−46.9, −52.7, −68.5) mm (right\left SUB, 5 mm^3). The left and right VOIs on STR, FC, SUB, and TSW were combined into single VOIs for each structure. The CB VOI (7.6 mm^3) consisted of a prolate ellipsoid centered at (−0.5, −46.5, −106.0) mm with a long axis of 3.6 mm and a short axis of 2 mm.

The dynamic PET images were first summed and the sum image was resliced using the Fusion toolbox of PMOD to match the size of the template. All sum images were subjected to an initial spatial transformation consisting of a scale factor (zoom) of 10 and a rotation of 180 degrees around the z axis so that the orientation of the brain to roughly match the orientation of the MR brain template. Through subsequent rigid transformations (translations and rotations) applied to each sum image the brain was co-registered to match the template and therefore the Paxinos atlas. The resulting transformation matrix for each subject was subsequently applied to all the images in the dynamic series. Time activity curves (TACs) were extracted for each VOI from the dynamic PET data.

The *ex vivo* images were also rescaled to match the template. However, due to the resulting decompression following the excision of the brain from the skull it was not possible to co-register the images to the template using a simple rigid transformation. However, the *ex vivo* PET images were manually co-registered to each other and unique VOIs were drawn on TH, STR, FC, SUB, TSW and CB. The same regions were also identified and drawn on the autoradiographic images, along with auditory cortex (AC) and auditory thalamus (medial geniculate, MG) identified from unstained tissue sections.

Mouse *in vivo* PET images also were co-registered to an MRI brain template (Ma et al., 2005) of size 192 x 96 x 256 voxels with a voxel size of 2 mm, which was preliminarily scaled by a factor of 20. VOIs representing TH and CB were manually drawn on the MR template and copied to PET images.

Kinetic analysis of rat *in vivo* PET studies was performed using kinetic analysis toolbox in PMOD. Distribution volume ratio (DVR) in each selected brain region was calculated for using Logan non-invasive method (LNI) (Logan et al., 1996). Binding potential (BP_{ND}) was calculated as “DVR-1.” Cerebellum was used as a reference region since it is known not

to be enriched with α4β2* nAChRs. LNI method requires prior estimation of the blood-tissue tracer transfer rate in the cerebellum, k'_2, which was computed indirectly from fitting the simplified reference tissue model (SRTM) (Lammertsma and Hume, 1996) to the TH curve using a Marquandt optimization algorithm with 200 iterations. The estimated k'_2 for each subject was then fixed and used subsequently for Logan analysis of all other brain regions. The cutoff of Logan plot was determined based on a preset error of 10% between the fit and the data.

In *ex vivo* analysis and autoradiography, ^{18}F-nifene binding was quantified as ratios between activity in the target region and that in the cerebellum.

Behavior experiments

Animals: Adult, male Sprague–Dawley rats (300–350 g, Charles River Laboratories; Wilmington, MA) were housed in individual cages in a temperature controlled (22° C) vivarium and maintained on a 12/12 h light/dark cycle (lights on at 7:00 a.m.) with *ad libitum* access to food and water. Animals were handled for 2–3 days before an adaptation session of 30 min free exploration in a shuttle box training apparatus.

Training apparatus and tone generation: Training was conducted in a shuttle box (modified from H10-11R-SC Coulbourn Instruments, Allentown, PA) contained within a sound-attenuating enclosure (H10-24A, Coulbourn). The shuttle box consisted of an alley-way contained by clear acrylic walls (51.0 cm long, 10.5 cm wide and 8.0 cm high) illuminated by two house lights (H11-01R, Coulbourn), and a centrally-located overhead speaker for presentation of tones (H12-01R, Coulbourn). The floor was an electrified grid that could deliver 8-pole scrambled foot shock (60 Hz, 0.7 mA; H13–15, Coulbourn) to either half of the shuttle box. Acoustic stimuli were 8.0 kHz tones (65 dB SPL, rise/fall time 5 ms, calibrated for animal head height throughout the alley), presented at the rate of 2.5 Hz (310 ms on alternating with 90 ms of silence) for 10 s, generated by Tucker-Davis Technologies (TDT) System 3 (RP2.1 Real-Time Processor) and RPvdsEx software. Tone and shock presentation, and behavioral responses were controlled and recorded with Coulbourn Graphic State software.

Training protocol: Prior to training with tones, animals were shaped to escape shock (e.g., Liang et al, 2008). The goal of shaping was to promote running to the opposite side of the shuttlebox to minimize receipt of shock, which was escaped upon crossing the midline. The shock was administered only when animals faced the opposite side. These shock-only trials were given on average at intervals of 60 ± 20 s. Shaping trials were presented until the animal learned to orient to the opposite side of the shuttle box, cross the midline when shocked and re-orient to face the other side in preparation for the next trial (maximum crossing latency, <60 s).

The first auditory-cued avoidance training session began immediately after escape training and consisted of 30 trials per daily session (inter-trial intervals, 60 ± 20 s). Each trial consisted of tone presentation that signaled forthcoming shock (tone onset-to-shock interval, 10 s). An avoidance response was defined as a midline crossing during the 10 s tone-shock interval, before the presentation of shock. Escape responses were crossings made after the 10 s tone-shock interval, during shock presentation. Tone presentation ceased at the moment of midline crossing. Crossings during the silent inter-trial intervals had no effect. Performance was measured as the percentage of avoidance responses during a session, i.e.: (number of trials with avoidance responses/number of trials) x 100%. Initial avoidance training was for 14 consecutive days. To confirm performance prior to imaging, short blocks of training were resumed in animals selected for imaging for a total of 21 training sessions over 2–3 months. Training was continued beyond 14 days for two reasons. First, it assured

the consistency of “good” or “poor” avoidance behavior prior to imaging and second, it was used to determine whether all animals were equally capable of learning, if only to some low level of performance, and would exhibit the expected learning effect of memory consolidation (*i.e.*, an increase in performance after a retention period without continued training). Consolidation was calculated as the change in each animal’s performance after 2 weeks without training between sessions 14 and 15, i.e.: (percent avoidance during session 15 – percent avoidance during session 14).

Results

We present the results in three sections. In Section 1, we demonstrate the selectivity of ^{18}F-nifene using wild-type (WT) and transgenic (β2 knockout, β2-KO) mice, show its distribution in rat forebrain using three methods—*in vivo* PET, *ex vivo* PET and autoradiography—and compare ^{18}F-nifene binding obtained using the three methods. The cerebellum (CB) exhibited minimal binding and served as a reference. Subsequent experiments were done only in the rat due to superior spatial resolution for imaging, and well-characterized behavior (see below). In Section 2, we describe the performance of 12 rats trained on an auditory-cognitive task, i.e., auditory-cued active avoidance. Performance on this task is impaired by lesions of auditory cortex (Delay and Rudolph, 1994; Duvel et al., 2001; Ohl et al., 1999), and enhanced by systemic administration of nicotine (Erickson, 1971; Sansone et al., 1994a; Sansone et al., 1994b; Sansone et al., 1991; Yilmaz et al., 1997). Finally, in Section 3, we present ^{18}F-nifene binding data for six rats—the three best-performing and three worst-performing animals from the cohort in Section 2—in order to correlate performance with binding in selected brain regions. Seven regions were selected for their relevance to auditory processing (auditory cortex, AC; auditory thalamus/medial geniculate, MG; and the intervening temporal subcortical white matter, TSW) and for known high levels of nAChRs (frontal cortex, FC; striatum, STR; subiculum, SUB; and overall thalamus, TH).

Section 1. Imaging ^{18}F-nifene: *in vivo* PET, *ex vivo* PET and autoradiography

PET imaging of anesthetized WT and β2-KO mice was carried out using ^{18}F-nifene. Fig. 1A–C includes coronal sections of mouse MR template (Fig. 1A) through TH and cortical regions. Binding of ^{18}F-nifene in the TH of the WT was observed (Fig. 1B) while the β2-KO mouse had minimal binding (Fig. 1C). Measured TH-to-CB ratios of ^{18}F-nifene in WT was 1.3 while that in the β2-KO was 0.92. In autoradiography, WT horizontal slices (Fig. 1D) exhibited ^{18}F-nifene binding in several brain regions consistent with our findings in rats (see below and (Easwaramoorthy et al., 2007). These regions included TH, STR, FC, SUB and CB. In contrast,β2-KO mice (Fig. 1E) showed little binding. Average TH-to-CB ratio in autoradiography tissue was 6.4 in WT and 2.1 in β2-KO mice. Using adjacent brain slices from the same mouse brains, dopamine D2/D3 receptors were imaged in STR in both WT and β2-KO (Fig. 1F, G) using ^{18}F-fallypride. ^{18}F-Fallypride imaging of WT and β2-KO mice revealed similar binding in STR (STR/CB = 13.7 for WT, 14.0 for β2-KO). In both individual examples and group data (Fig. 1H, n = 2), WT mice exhibited the binding profile for ^{18}F-nifene of TH > SUB ≈ STR ≈ FC > HP ≈ CB and for ^{18}F-fallypride of STR > TH > FC > HP ≈ CB, whereas β2-KO mice revealed ^{18}F-fallypride binding consistent with the WT, but had little ^{18}F-nifene binding. ^{18}F-Nifene binding in WT mice was greater than in β2-KO mice in all regions (paired one-tailed t-test, df 2, n= 2, $p < 0.01$). Binding of ^{18}F-fallypride in STR of WT mice was not different from that in STR of β2-KO mice ($p = 0.45$).

We then examined localization of ^{18}F-nifene in rat using co-registered PET images and the rat brain MRI template (Fig. 2, top row). Figure 2 (middle row) shows horizontal PET

sections with ^{18}F-nifene binding measured in regions corresponding to those on the MRI template. The fused images (Fig. 2, bottom) confirm good co-registration of major landmarks such as FC, TH and CB, consistent with our previous work using an MRI template (Constantinescu et al., 2011).

Representative time-activity curves of ^{18}F-nifene are shown in Fig. 3. Curves were generated for TH, STR, FC, SUB, TSW and CB. TH exhibited the highest binding followed by other brain regions consistent with previous findings in rat and monkey (Kant et al., 2011; Pichika et al., 2006). Note that the time-activity curve of TSW was suggestive of significant receptor-mediated binding, similar to that of FC and SUB. Average binding potentials (BP_{ND}) varied between 1.97 for TH and 0.66 for STR and followed the order TH > SUB > FC > TSW > STR (see Table 1).

Following the 90-min *in vivo* PET scan, the brain of each rat was immediately excised and *ex vivo* PET images were acquired. Distribution of ^{18}F-nifene was consistent across animals and brain regions. Figure 4A shows an example of an *ex vivo* PET image with maximum binding in TH, followed by FC, STR and TSW, with little binding in CB. After the *ex vivo* PET scan, horizontal brain sections (20 μm) were cut for autoradiography. Brain sections (Fig. 4B) showed ^{18}F-nifene relative binding consistent with that seen in PET images. For quantitative measurements, photoscans of tissue sections were used to identify brain regions (Fig. 4C). Note, in Fig. 4B, bilateral binding of ^{18}F-nifene in the TSW between TH and temporal cortex (additional details below). The order of ^{18}F-nifene binding among the various regions largely followed that measured in PET scans (TH > SUB > FC > TSW > STR > CB).

Quantitative analysis of ^{18}F-nifene binding using the three imaging methods is shown in Table 1. For each method, CB was used as a reference region. The *ex vivo* measures (PET and autoradiography) are direct ratios while the *in vivo* measure is a BP_{ND} derived from distribution volume ratios (DVR-1) obtained from the analysis of dynamic PET data. The rank order of ^{18}F-nifene binding across brain regions for the three methods followed a similar profile. Identification of regions of interest, particularly small brain regions such as the SUB and TSW, were more accurate in the higher-resolution autoradiographs (cf. Figs. 2 and 4). While both *in vivo* and *ex vivo* measurements were aided by MRI template fused images, fusion of the excised brain was more challenging due to small changes in gross structure (e.g., caused by compression of the excised brain), affecting quantitation of smaller brain regions.

Figure 5 shows the correlation between autoradiography and *ex vivo* PET (Fig. 5A) or *in vivo* PET (Fig. 5B), after averaging data across animals (n = 6; binding in CB used to normalize values across animals). For these measures of average binding, the correlations between methods were high (Fig. 5A, $r^2 = 0.972$, $p = 0.002$; Fig. 5B, $r^2 = 0.935$, $p = 0.007$). However, binding in specific brain regions of individual animals did not always correlate well among measurement methods, likely due to methodological limitations, e.g., imaging in small brain regions using either PET method (Fig. 5C, example of correlation between autoradiography and *in vivo* PET measures for TSW binding, $r^2 = 0.448$, $p = 0.146$; values for other pairwise comparisons with autoradiography ranged from $r^2 = 0.027$ for *in vivo* PET SUB to $r^2 = 0.953$ for *ex vivo* PET TH). Thus, while averaging across animals yields good agreement among methods, only the highest resolution method, autoradiography, was used for comparison of ^{18}F-nifene binding among individual animals (Section 3, below).

Given the apparent ^{18}F-nifene binding in TSW (Fig. 4), we also compared binding in several prominent white matter tracts: corpus callosum, fimbria, TSW and cerebellar white matter (Fig. 6A). For the example (Fig. 6B) and group (Fig. 6E) autoradiograph data in Fig. 6,

binding was highest in TSW, followed by fimbria, corpus callosum (CC) and cerebellar white matter (CBW; note, however, that spillover into the fimbria from the adjacent TH and STR probably results in an overestimation of activity). For both autoradiography and *ex vivo* PET results, ^{18}F-nifene binding differed among white matter regions (Fig. 6E, ANOVAs, $p < 0.01$; *post-hoc* Tukey-Kramer pair-wise comparisons indicated TSW differed from all other regions for autoradiography, and that all regions differed from each other for *ex vivo* PET). Nonspecific binding was determined by autoradiography after displacement from nAChRs by 300 mM nicotine (Fig. 6C–D). ^{18}F-Nifene binding in CC, fimbria and TSW was reduced following nicotine displacement (Fig. 6E, one-tailed t-test, n = 2–3, p = 0.0001, 0.0010, 0.0.0039, respectively) while binding in CBW was not reduced (p = 0.1378). These data indicate significant ^{18}F-nifene binding in white matter, notably TSW.

Section 2. Auditory behavior

A group of 12 male rats underwent behavioral training for 14 days (30 trials per day). Each was placed in a shuttle box where a tone signaled an impending shock (beginning 10 s after tone onset). Crossing the midline terminated the tone (if the animal crossed <10 s after tone onset) or concurrent tone and shock (if the animal crossed >10 s after tone onset). With training, over half the animals (7/12) learned to avoid the shock by crossing to the other compartment in time. The remaining animals (5/12) on most trials did not cross in time, and escaped the shock by crossing only after shock onset. Performance for the 12 animals is shown in Fig. 7 (inset). Mean avoidance performance across the 14-day block of training provided a criterion to designate an individual subject's learning as "good" (above the group mean) or "poor" (below the mean). Of the 12 trained animals, six that represented extreme levels of good (n = 3) and poor (n = 3) learning were selected for subsequent imaging; their performance is shown in Fig. 7.

The three good and three poor learners exhibited avoidance performance above 90% or below 10%, respectively, in at least one of the first five training sessions. Across avoidance training sessions, there was a significant difference in performance between groups: ($F_{(20,84)} = 2.91$, $p < 0.0003$). All animals were tested two weeks after the end of training to confirm lasting effects (Fig. 7, Consolidation), and once more after a variable interval (depending on availability of the scanner), immediately prior to imaging (Fig. 7, Pre-Scan). The good learners showed an increase in avoidance performance after the 2-week consolidation period of 11.1 ± 6.2%, which might have been greater but for a ceiling effect. Of particular interest, the poor learners also exhibited an increase in avoidance of 34.4 ± 18.5%. Thus, they were capable of learning the task, albeit not as well as the good performers, and their mechanisms for memory consolidation were functional.

The difference in group performance (good vs. poor learners) was not due to a difference in ability to cross the midline to the safe side of the shuttlebox, since the ability to escape shock did not differ between groups: shock levels were not different (*Mann-Whitney U* = 8.0, p = 0.40), the number of shock escape shaping trials was not different (median ± inter-quartile range): good (8 ± 3) vs. poor (10 ± 15), *Mann-Whitney U* = 8.5, p = 0.50), and the latency to escape shock was not different (median ± inter-quartile range): good (15.5 sec ± 15.8) vs. poor (28.3 sec ± 34.9); *Mann-Whitney U* = 13.0, p = 0.40). Therefore, differences in avoidance performance appear to reflect differences in learning ability in this task, rather than differences in ability to perform the avoidance response.

Section 3. Correlation of ^{18}F-nifene binding with behavior

The six best and worst learners were placed in the PET scanner and imaged for ^{18}F-nifene binding using *in vivo* PET, *ex vivo* PET and autoradiography. The imaging data is presented above (Section 1), but because of the high spatial resolution and reliability of

autoradiography, only it was correlated with behavior. The extent of ^{18}F-nifene binding was measured in the five regions described above (e.g., Fig. 4), plus AC and MG as identified from photoscans of autoradiography sections (e.g., Fig. 4C). Thus, the seven brain regions chosen for analysis include three from the auditory forebrain (AC, MG and TSW), and four regions characterized by significant ^{18}F-nifene binding (TH, FC, SUB and STR). For each region, ^{18}F-nifene binding was correlated with performance on the auditory-cued behavioral task. Performance was characterized using multiple measures including learning rate, eventual level of performance after 14 days training, and subsequent performance at the 2-week retention test (Table II). Significant correlations between the performance and ^{18}F-nifene binding are indicated in Table II (regression coefficient, r, values, *$p < 0.05$, or **$p < 0.01$). Two notable brain regions are FC and TSW; for each of these regions, ^{18}F-nifene binding correlates with all, or nearly all, behavioral measures. Figure 8 depicts representative scatter plots relating ^{18}F-nifene binding in each of the regions to learning rate (column 1 in Table II).

To demonstrate how ^{18}F-nifene binding determined after training relates to the development of behavior over the period of training, Fig. 9 shows the correlation of binding in each brain region with the level of avoidance performance on each day of training (gray shading in Fig. 9 indicates significant correlation). Of the 7 brain regions, only TH shows significant correlations for each of the first 2 days of training, but the correlation decreases thereafter over the 2 weeks. Conversely, TSW, SUB and FC show significant correlations only on the third day or later, with FC reaching criterion only on the last day. Other brain regions, notably AC and MG in the auditory forebrain, never showed significant correlation of ^{18}F-nifene binding with performance.

The contrast in Fig. 9 between TH (higher correlation early in training) and FC, SUB and TSW (higher correlation later in training), suggests the possibility that nAChRs in different brain regions contribute to behavior during different phases of learning. An analysis suggesting differential involvement of brain regions over the course of training is shown in Fig. 10: pairs of regions that correlate similarly with behavior throughout training show positive regressions – for example, TSW and SUB show similarly poor correlations between ^{18}F-nifene binding and performance on days 1–2, and increasingly better correlations over the next 12 days – whereas the opposite trend (negative-slope regression) is seen when correlating TH with other regions. The negative regressions suggest a systematic transition from brain networks involving TH to those involving other regions (TSW, FC, SUB).

Discussion

We examined the distribution of ^{18}F-nifene in behaviorally-characterized rats, in order to relate the availability of nAChRs in forebrain sub-regions to behavioral performance. Three imaging methods—*in vivo* PET, *ex vivo* PET and autoradiography—produced similar measures of relative binding of ^{18}F-nifene among brain regions, and the overall distribution was consistent with that of α4β2* nAChRs, as was the lack of binding in β2-KO mice. An important finding was that ^{18}F-nifene labeled some white matter pathways, notably the TSW containing the auditory thalamocortical pathway. Finally, a comparison of ^{18}F-nifene binding with auditory-cued behavior produced four regions with significant correlations: TSW, FC, SUB and TH. Binding in other areas, notably AC and MG in the auditory forebrain, did not correlate with behavior.

^{18}F-nifene binding in rat forebrain

The distribution of ^{18}F-nifene in the present study is consistent with previous results suggesting that ^{18}F-nifene binds to α4β2* nAChRs (Easwaramoorthy et al., 2007; Kant et al., 2011; Pichika et al., 2006). Lack of binding in the β2-KO mouse further supports this conclusion. All three methods of quantifying ^{18}F-nifene binding—*in vivo* PET, *ex vivo* PET and autoradiography—show the same order of relative binding among brain subregions, supporting the utility of each method. However, in individual animals, between-method comparison of measurements for some brain regions did not produce strong correlations. This may reflect methodological limits, especially for regions with low levels of ^{18}F-nifene binding, and is less of an issue for regions with higher levels; in TH, for example, repeated PET measurements in the same animal vary only ~3% (Kant et al., 2011). Thus, while the finding of similar relative binding among brain regions is likely due to averaging across animals, only the highest resolution method—autoradiography—was used for correlating binding with behavior in individual animals.

A notable finding is that of ^{18}F-nifene in the white matter pathway between the dorsal thalamus and temporal cortex, i.e., the TSW. A similar conclusion was reached in a PET study of α4β2* nAChRs in humans (Ding et al., 2004). In that study, as in the present one, weaker binding was observed in other white matter pathways, such as corpus callosum. Ding et al. (2004) note that binding in white matter is not necessarily functional, but may, for example, reflect axonal transport of nAChRs. However, recent work suggests that activation of nAChRs in the auditory thalamocortical pathway enhances the excitability of myelinated thalamocortical axons (Kawai et al., 2007). Moreover, microinjection of nAChR antagonist into the pathway reduced the amplitude of sound-evoked responses in auditory cortex, suggesting that endogenously released ACh acts at nAChRs in the pathway to enhance cortical responsiveness. Thus, ACh release upon increased arousal and attention could enhance sound-evoked responses in A1. Conversely, studies of chronic nicotine exposure in smokers or their offspring have revealed deficits in auditory function and TSW structure (Fried et al., 2003; Jacobsen et al., 2007a; Jacobsen et al., 2007b; McCartney et al., 1994). These effects, both positive and negative, may involve nAChRs situated along TSW pathways.

^{18}F-nifene and behavior: relevance of nAChRs for cognitive function

Significant correlations were found between behavioral performance and ^{18}F-nifene binding in TSW, FC, TH and SUB. Each of these sites may contribute to performance in the behavioral task. Given the auditory nature of the task, TSW binding may indicate that activation of nAChRs in the auditory thalamocortical pathway could increase thalamocortical relay of acoustic information and produce stronger cortical responses, which could underlie better performance. Such a mechanism is consistent with our prior finding that animals with better performance (using the same task as in the present study) exhibit stronger nicotinic enhancement of tone-evoked cortical responses(Liang et al., 2008). It is important to note, however, that the TSW includes not only thalamocortical axons but also corticothalamic projections. Moreover, it is not clear exactly where nAChRs are situated and what they regulate; while changes in axon excitability might be expected to involve nodes of Ranvier, the dense TSW binding in some animals seems to imply binding that extends beyond just nodes. Non-neuronal binding sites, for example on astrocytes, may also regulate neuronal function (Grybko et al., 2010; Hernandez-Morales and Garcia-Colunga, 2009). Regardless of the locus of action, behaviorally-induced regulation of TSW might contribute to lasting changes, such as those observed in white matter pathways following behavioral training (Carreiras et al., 2009; Scholz et al., 2009). Finally, it is important to note that the involvement of TSW in the present study could not have been observed with standard

electrophysiological or metabolic approaches, underscoring the novelty and utility of ^{18}F-nifene imaging.

There was no correlation of performance with binding in other auditory forebrain regions, i.e., MG and AC. This lack of correlation does not necessarily mean that nAChRs in these structures are not important for performance, but potentially that nAChRs contribute multiple functions, some of which may not be related to performance on this task.

The measured region in the FC corresponds closely to the medial prefrontal cortex (mPFC) (cf. VOI in Fig. 2) (Paxinos and Watson, 1986), which has been implicated in executive control of processing in auditory and other sensory cortices (Hasselmo and Sarter, 2011; Romanski et al., 1999), and which has reciprocal connections with basal forebrain and brainstem cholinergic nuclei (Uylings et al., 2003). In particular, mPFC is thought to regulate sensory cortex by way of nucleus basalis cholinergic neurons (Hasselmo and Sarter, 2011; Parikh et al., 2007). Moreover, nAChRs are known to regulate multiple thalamocortical and intrinsic circuits within the mPFC (Lambe et al., 2003; Poorthuis et al., 2009), thereby contributing to its attention-related functions (Hahn et al., 2003). It is likely that some of these circuits contribute to the behavioral outcomes observed in the present study.

Two other regions, TH and SUB, also were implicated in nicotinic regulation of behavior. The implication of SUB is consistent with its role in nicotinic regulation of information flow through the hippocampal-entorhinal complex, a critical locus for cognitive function (O'Mara, 2005; Perry et al., 2002; Tu et al., 2009). SUB also is an interface with PFC and brain reward centers such as nucleus accumbens (Cooper et al., 2006). Alone of all measured brain regions, TH binding correlated well with performance on the first two days of training, but the correlation declined over the remaining period of training even as it increased for other regions (TSW, FC and SUB). This result suggests that nicotinic regulation of TH is most important early in training, and that there is a systematic progression, as training continues, to nicotinic regulation in other brain regions. This progression resembles a similar transition over time of memory-related substrates from hippocampus to cerebral cortex in other tasks (Bontempi et al., 1999). The current findings support a transition from TH to TSW, FC and SUB for improved levels of performance over the course of training, and also regional specificity of nicotinic regulation in these latter areas to support learning-related behaviors like the rate of acquisition and successful memory retention.

These results support the use of ^{18}F-nifene for relating nAChRs to behavior, and potentially for tracking the dynamics of brain networks during learning acquisition and memory consolidation. The use of PET, in particular, raises the possibility of assessing nAChR availability repeatedly across training, for example, to examine whether better performance is the result of, or results from, increased nAChR availability. Our findings support the feasibility of before-and-after PET imaging, especially in larger brain regions and larger brains. Notably, given the advantages of ^{18}F-nifene over radioligands currently used for human PET studies (i.e., significantly shorter scan times), future investigations could examine this important issue in humans. Overall, our findings suggest that individual performance is linked to nicotinic functions in specific brain regions, and further support a role for nAChRs in sensory-cognitive function.

Acknowledgments

This work was supported by NIH grants R01AG029479 (JM), R01DC02938, R01DC010013 (NMW), DC009163 (KMB), RO3DC08204 (HDK) and R01DA12929, P30DC08369 (RM). We thank Robert Coleman for technical assistance, and Dr. Marina Picciotto for providing breeding stock for β2 knock-out mice.

References

Bao Q, Newport D, Chen M, Stout DB, Chatziioannou AF. Performance evaluation of the inveon dedicated PET preclinical tomograph based on the NEMA NU-4 standards. J Nucl Med. 2009; 50(3):401–408. [PubMed: 19223424]

Bontempi B, Laurent-Demir C, Destrade C, Jaffard R. Time-dependent reorganization of brain circuitry underlying long-term memory storage. Nature. 1999; 400(6745):671–675. [PubMed: 10458162]

Carreiras M, Seghier ML, Baquero S, Estevez A, Lozano A, Devlin JT, Price CJ. An anatomical signature for literacy. Nature. 2009; 461(7266):983–986. [PubMed: 19829380]

Constantinescu CC, Coleman RA, Pan ML, Mukherjee J. Striatal and extrastriatal microPET imaging of D2/D3 dopamine receptors in rat brain with [(1)F]fallypride and [(1)F]desmethoxyfallypride. Synapse. 2011; 65(8):778–787. [PubMed: 21218455]

Constantinescu CC, Mukherjee J. Performance evaluation of an Inveon PET preclinical scanner. Phys Med Biol. 2009; 54(9):2885–2899. [PubMed: 19384008]

Cooper DC, Klipec WD, Fowler MA, Ozkan ED. A role for the subiculum in the brain motivation/reward circuitry. Behav Brain Res. 2006; 174(2):225–231. [PubMed: 16870273]

Delay ER, Rudolph TL. Crossmodal training reduces behavioral deficits in rats after either auditory or visual cortex lesions. Physiol Behav. 1994; 55(2):293–300. [PubMed: 8153168]

Ding YS, Fowler JS, Logan J, Wang GJ, Telang F, Garza V, Biegon A, Pareto D, Rooney W, Shea C, Alexoff D, Volkow ND, Vocci F. 6-[18F]Fluoro-A-85380, a new PET tracer for the nicotinic acetylcholine receptor: studies in the human brain and in vivo demonstration of specific binding in white matter. Synapse. 2004; 53(3):184–189. [PubMed: 15236351]

Duvel AD, Smith DM, Talk A, Gabriel M. Medial geniculate, amygdalar and cingulate cortical training-induced neuronal activity during discriminative avoidance learning in rabbits with auditory cortical lesions. J Neurosci. 2001; 21(9):3271–3281. [PubMed: 11312312]

Easwaramoorthy B, Pichika R, Collins D, Potkin SG, Leslie FM, Mukherjee J. Effect of acetylcholinesterase inhibitors on the binding of nicotinic alpha4beta2 receptor PET radiotracer, (18)F-nifene: A measure of acetylcholine competition. Synapse. 2007; 61(1):29–36. [PubMed: 17068780]

Erickson CK. Studies on the mechanism of avoidance facilitation by nicotine. Psychopharmacologia. 1971; 22(4):357–368. [PubMed: 5133437]

Espeseth T, Sneve MH, Rootwelt H, Laeng B. Nicotinic Receptor Gene CHRNA4 Interacts with Processing Load in Attention. PloS one. 2010; 5(12):e14407. [PubMed: 21203548]

Fried PA, Watkinson B, Gray R. Differential effects on cognitive functioning in 13- to 16-year-olds prenatally exposed to cigarettes and marihuana. Neurotoxicol Teratol. 2003; 25(4):427–436. [PubMed: 12798960]

Grybko M, Sharma G, Vijayaraghavan S. Functional distribution of nicotinic receptors in CA3 region of the hippocampus. J Mol Neurosci. 2010; 40(1–2):114–120. [PubMed: 19693709]

Hahn B, Shoaib M, Stolerman IP. Involvement of the prefrontal cortex but not the dorsal hippocampus in the attention-enhancing effects of nicotine in rats. Psychopharmacology (Berl). 2003; 168(3):271–279. [PubMed: 12698230]

Hasselmo ME, Sarter M. Modes and models of forebrain cholinergic neuromodulation of cognition. Neuropsychopharmacology. 2011; 36(1):52–73. [PubMed: 20668433]

Hernandez-Morales M, Garcia-Colunga J. Effects of nicotine on K+ currents and nicotinic receptors in astrocytes of the hippocampal CA1 region. Neuropharmacology. 2009; 56(6–7):975–983. [PubMed: 19371581]

Hillmer AT, Wooten DW, Moirano J, Slesarev M, Barnhart TE, Engle JW, Nickles RJ, Murali D, Schneider M, Mukherjee J, Cristian BT. Specific alpha4-beta2 nicotinic acetylcholine receptor binding of [F-18]nifene in the rhesus monkey. Synapse. 2011 in press.

Horti AG, Gao Y, Kuwabara H, Dannals RF. Development of radioligands with optimized imaging properties for quantification of nicotinic acetylcholine receptors by positron emission tomography. Life Sci. 2010; 86(15–16):575–584. [PubMed: 19303028]

Jacobsen LK, Picciotto MR, Heath CJ, Frost SJ, Tsou KA, Dwan RA, Jackowski MP, Constable RT, Mencl WE. Prenatal and adolescent exposure to tobacco smoke modulates the development of white matter microstructure. J Neurosci. 2007a; 27(49):13491–13498. [PubMed: 18057207]

Jacobsen LK, Slotkin TA, Mencl WE, Frost SJ, Pugh KR. Gender-specific effects of prenatal and adolescent exposure to tobacco smoke on auditory and visual attention. Neuropsychopharmacology. 2007b; 32(12):2453–2464. [PubMed: 17375135]

Kant R, Constantinescu CC, Parekh P, Pandey SK, Pan M-L, Easwaramoorthy B, Mukherjee J. Evaluation of 18F-nifene binding to α4β2 nicotinic receptors in the rat brain using microPET imaging. EJNMMI Research. 2011; 1(1):6.

Kawai H, Lazar R, Metherate R. Nicotinic control of axon excitability regulates thalamocortical transmission. Nat Neurosci. 2007; 10(9):1168–1175. [PubMed: 17704774]

Lambe EK, Picciotto MR, Aghajanian GK. Nicotine induces glutamate release from thalamocortical terminals in prefrontal cortex. Neuropsychopharmacol. 2003; 28:216–225.

Lammertsma AA, Hume SP. Simplified reference tissue model for PET receptor studies. Neuroimage. 1996; 4(3 Pt 1):153–158. [PubMed: 9345505]

Levin ED, McClernon FJ, Rezvani AH. Nicotinic effects on cognitive function: behavioral characterization, pharmacological specification, and anatomic localization. Psychopharmacology (Berl). 2006; 184(3–4):523–539. [PubMed: 16220335]

Li JG, Lehr M, Liu-Chen LY, Woodruff-Pak DS. Nicotinic acetylcholine receptors and modulation of learning in 4- and 27-month-old rabbits. Neuropsychopharmacology. 2008; 33(12):2820–2830. [PubMed: 18256594]

Liang K, Poytress BS, Weinberger NM, Metherate R. Nicotinic modulation of tone-evoked responses in auditory cortex reflects the strength of prior auditory learning. Neurobiol Learn Mem. 2008; 90(1):138–146. [PubMed: 18378471]

Logan J, Fowler JS, Volkow ND, Wang GJ, Ding YS, Alexoff DL. Distribution volume ratios without blood sampling from graphical analysis of PET data. J Cereb Blood Flow Metab. 1996; 16(5):834–840. [PubMed: 8784228]

Ma Y, Hof PR, Grant SC, Blackband SJ, Bennett R, Slatest L, McGuigan MD, Benveniste H. A three-dimensional digital atlas database of the adult C57BL/6J mouse brain by magnetic resonance microscopy. Neuroscience. 2005; 135(4):1203–1215. [PubMed: 16165303]

McCartney JS, Fried PA, Watkinson B. Central auditory processing in school-age children prenatally exposed to cigarette smoke. Neurotoxicol Teratol. 1994; 16:269–276. [PubMed: 7935260]

Metherate R. Functional connectivity and cholinergic modulation in auditory cortex. Neurosci Biobehav Rev. 2011; 35(10):2058–2063. [PubMed: 21144860]

O'Mara S. The subiculum: what it does, what it might do, and what neuroanatomy has yet to tell us. Journal of anatomy. 2005; 207(3):271–282. [PubMed: 16185252]

Ohl FW, Wetzel W, Wagner T, Rech A, Scheich H. Bilateral ablation of auditory cortex in Mongolian gerbil affects discrimination of frequency modulated tones but not of pure tones. Learn Mem. 1999; 6(4):347–362. [PubMed: 10509706]

Parikh V, Kozak R, Martinez V, Sarter M. Prefrontal acetylcholine release controls cue detection on multiple timescales. Neuron. 2007; 56(1):141–154. [PubMed: 17920021]

Paxinos, G.; Watson, C. The Rat Brain in Stereotaxic Coordinates. New York: Academic Press; 1986.

Perry DC, Xiao Y, Nguyen HN, Musachio JL, Davila-Garcia MI, Kellar KJ. Measuring nicotinic receptors with characteristics of alpha4beta2, alpha3beta2 and alpha3beta4 subtypes in rat tissues by autoradiography. J Neurochem. 2002; 82(3):468–481. [PubMed: 12153472]

Perry E, Martin-Ruiz C, Lee M, Griffiths M, Johnson M, Piggott M, Haroutunian V, Buxbaum JD, Nasland J, Davis K, Gotti C, Clementi F, Tzartos S, Cohen O, Soreq H, Jaros E, Perry R, Ballard C, McKeith I, Court J. Nicotinic receptor subtypes in human brain ageing, Alzheimer and Lewy body diseases. Eur J Pharmacol. 2000; 393(1–3):215–222. [PubMed: 10771016]

Picciotto MR, Zoli M, Lena C, Bessis A, Lallemand Y, Le Novere N, Vincent P, Pich EM, Brulet P, Changeux JP. Abnormal avoidance learning in mice lacking functional high-affinity nicotine receptor in the brain. Nature. 1995; 374(6517):65–67. [PubMed: 7870173]

Pichika R, Easwaramoorthy B, Collins D, Christian BT, Shi B, Narayanan TK, Potkin SG, Mukherjee J. Nicotinic alpha4beta2 receptor imaging agents: part II. Synthesis and biological evaluation of 2-

[18F]fluoro-3-[2-((S)-3-pyrrolinyl)methoxy]pyridine (18F-nifene) in rodents and imaging by PET in nonhuman primate. Nuclear medicine and biology. 2006; 33(3):295–304. [PubMed: 16631077]

Poorthuis RB, Goriounova NA, Couey JJ, Mansvelder HD. Nicotinic actions on neuronal networks for cognition: general principles and long-term consequences. Biochem Pharmacol. 2009; 78(7):668–676. [PubMed: 19426718]

Romanski LM, Tian B, Fritz J, Mishkin M, Goldman-Rakic PS, Rauschecker JP. Dual streams of auditory afferents target multiple domains in the primate prefrontal cortex. Nat Neurosci. 1999; 2(12):1131–1136. [PubMed: 10570492]

Sansone M, Battaglia M, Castellano C. Effect of caffeine and nicotine on avoidance learning in mice: lack of interaction. J Pharm Pharmacol. 1994a; 46(9):765–767. [PubMed: 7837048]

Sansone M, Battaglia M, Vetulani J. Shuttle-box avoidance behavior of mice treated with nifedipine in combination with nicotine or physostigmine. Pol J Pharmacol. 1994b; 46(3):169–173. [PubMed: 8000449]

Sansone M, Castellano C, Battaglia M, Ammassari-Teule M. Effects of oxiracetam-nicotine combinations on active and passive avoidance learning in mice. Pharmacol Biochem Behav. 1991; 39(1):197–200. [PubMed: 1924503]

Scholz J, Klein MC, Behrens TE, Johansen-Berg H. Training induces changes in white- matter architecture. Nat Neurosci. 2009; 12(11):1370–1371. [PubMed: 19820707]

Schweinhardt P, Fransson P, Olson L, Spenger C, Andersson JL. A template for spatial normalisation of MR images of the rat brain. J Neurosci Methods. 2003; 129(2):105–113. [PubMed: 14511814]

Tu B, Gu Z, Shen JX, Lamb PW, Yakel JL. Characterization of a nicotine-sensitive neuronal population in rat entorhinal cortex. J Neurosci. 2009; 29(33):10436–10448. [PubMed: 19692619]

Uylings HB, Groenewegen HJ, Kolb B. Do rats have a prefrontal cortex? Behav Brain Res. 2003; 146(1–2):3–17. [PubMed: 14643455]

Yilmaz O, Kanit L, Okur BE, Pogun S. Effects of nicotine on active avoidance learning in rats: sex differences. Behav Pharmacol. 1997; 8(2–3):253–260. [PubMed: 9833020]

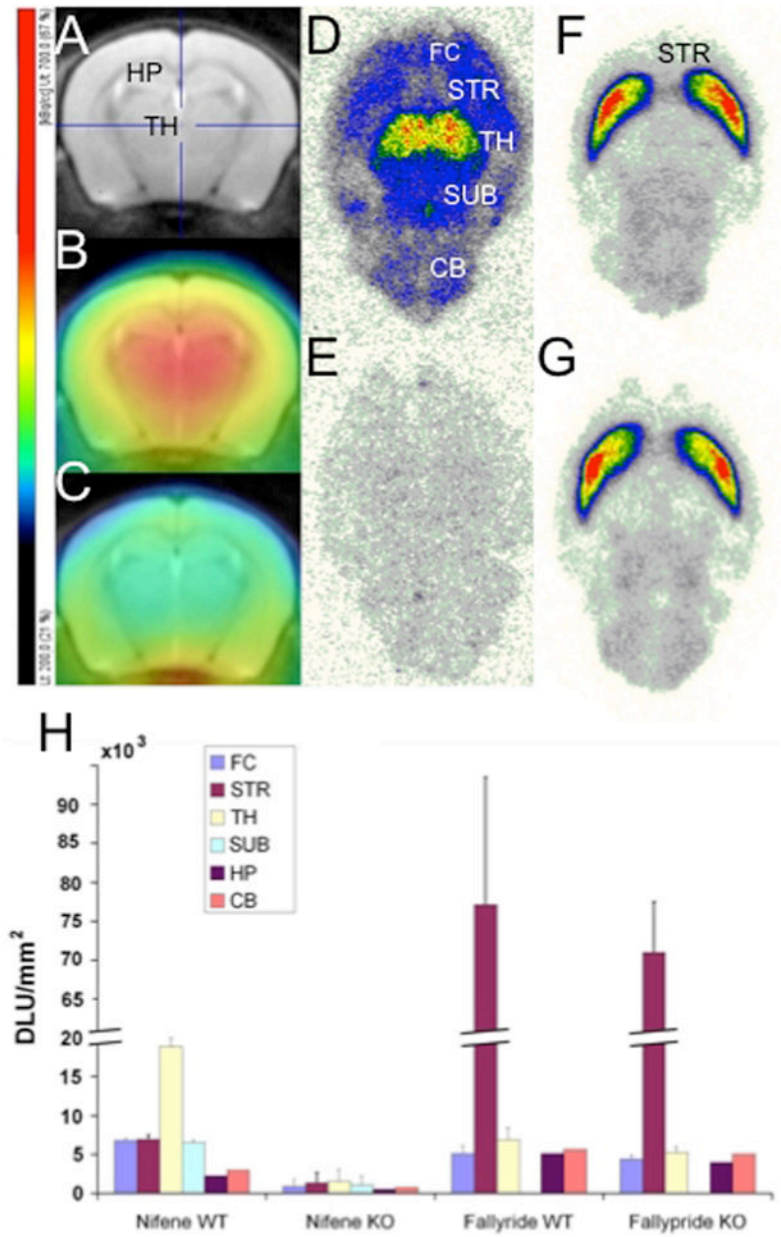

Figure 1.

^{18}F-Nifene and ^{18}F-fallypride binding in WT and β2-KO mouse brains. (A) Coronal slice from MR template of the mouse brain. (B, C) PET images showing strong ^{18}F-nifene binding in WT mouse (B) with little binding in β2-KO mouse (C). Color scale (left) reflects *in vivo* PET ^{18}F-nifene binding. (D–G) Mouse autoradiography horizontal slices showing ^{18}F-nifene binding in TH and other brain regions of WT (D), while β2-KO (E) showed little binding. In the same brain, as a control, ^{18}F-fallypride binds to dopamine D2/D3 receptors similarly in WT (F) and β2-KO (G). (H) Group data of ^{18}F-nifene and ^{18}F-fallypride binding in WT and β2-KO mouse brains (n = 2 each, multiple sections per animal); relative ^{18}F-nifene binding in TH > SUB ≈ STR ≈ FC > CB ≈ Hippocampus (HP), with little binding in β2-KO. ^{18}F-Fallypride binding was similar in WT and β2-KO. DLU/mm^2, digital light units per unit area (measured in autoradiographic sections, D–G).

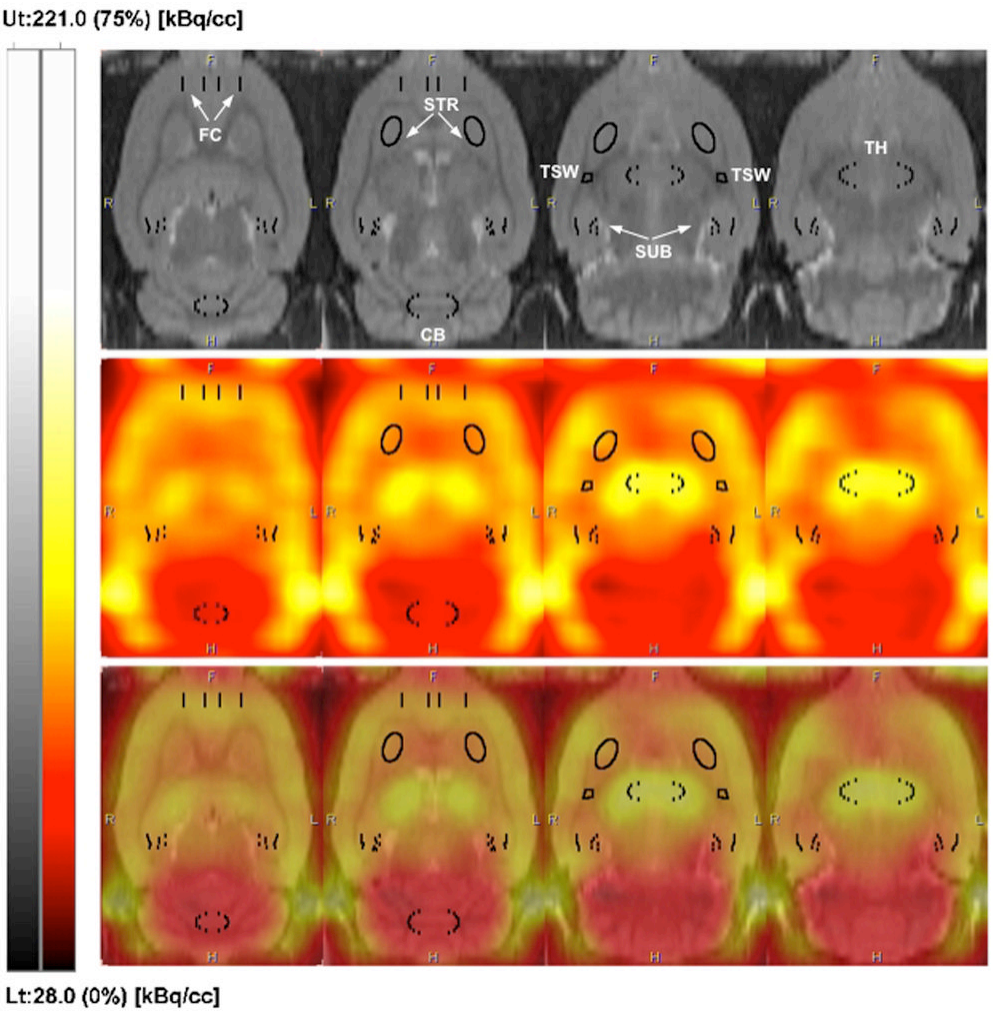

Figure 2.

PET imaging of ^{18}F-nifene in rat brain. Representative horizontal sections of a rat brain MR template (upper panel), *in vivo* PET imaging of ^{18}F-nifene (middle panel) and fused images (lower panel); coordinates with respect to bregma (left to right): −3.6, −4.4, −5.4 and −6.0 mm. PET images were integrated over 5–30 min interval, and the intensity was scaled relative to the whole image volume (upper threshold set to 75%). VOI placements on FC, STR, SUB, TSW and CB are shown on each panel, with labels on MR template. VOIs for TSW and STR were placed on the horizontal slices of the MR template. All other VOIs were placed on the axial slices.

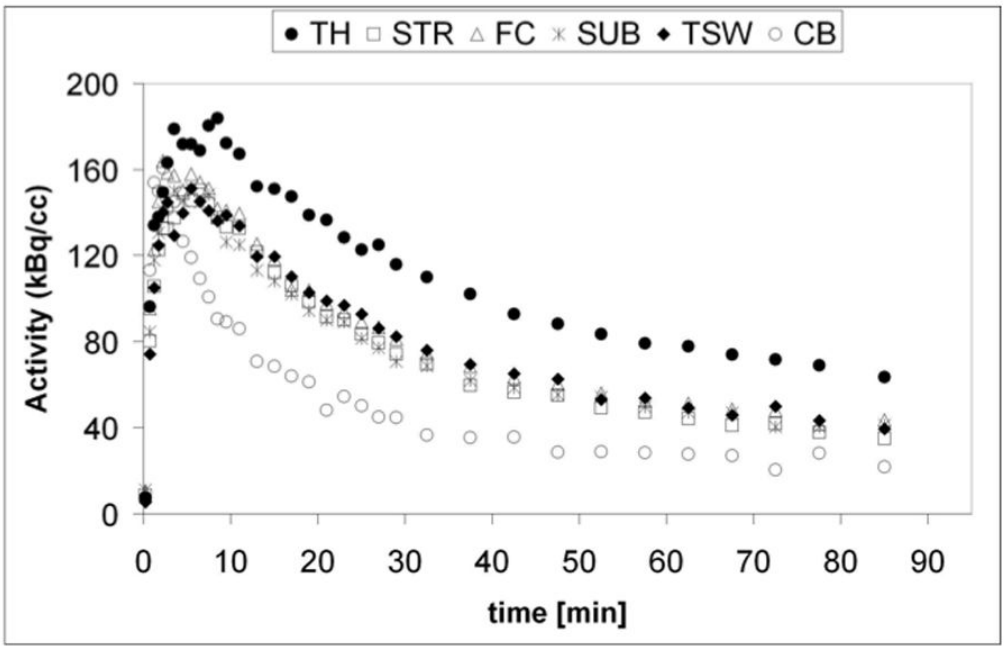

Figure 3.
Representative time-activity curves from an *in vivo* ^{18}F-nifene PET scan are shown for TH, STR, FC, SUB, TSW and CB.

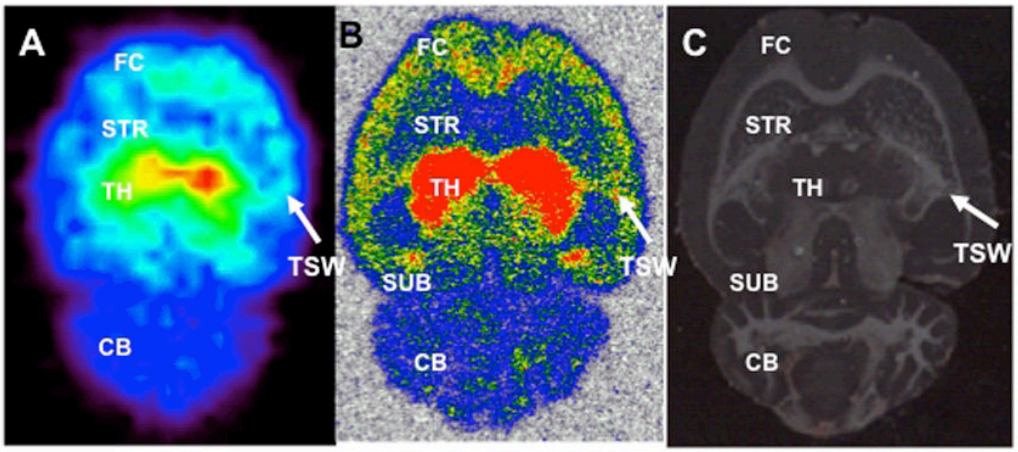

Figure 4.
^{18}F-nifene binding from horizontal *ex vivo* PET and autoradiography images in same rat brain. (A) *Ex vivo* PET image of a rat sacrificed 60 min after initial scan and the brain excised; maximum binding is in TH, lesser binding in FC, STR and TSW, and little binding in CB. (B) Autoradiograph of brain slice (40 μm) at level corresponding to the auditory forebrain shows prominent binding in TSW bilaterally. (C) Photoscan of same tissue section as B.

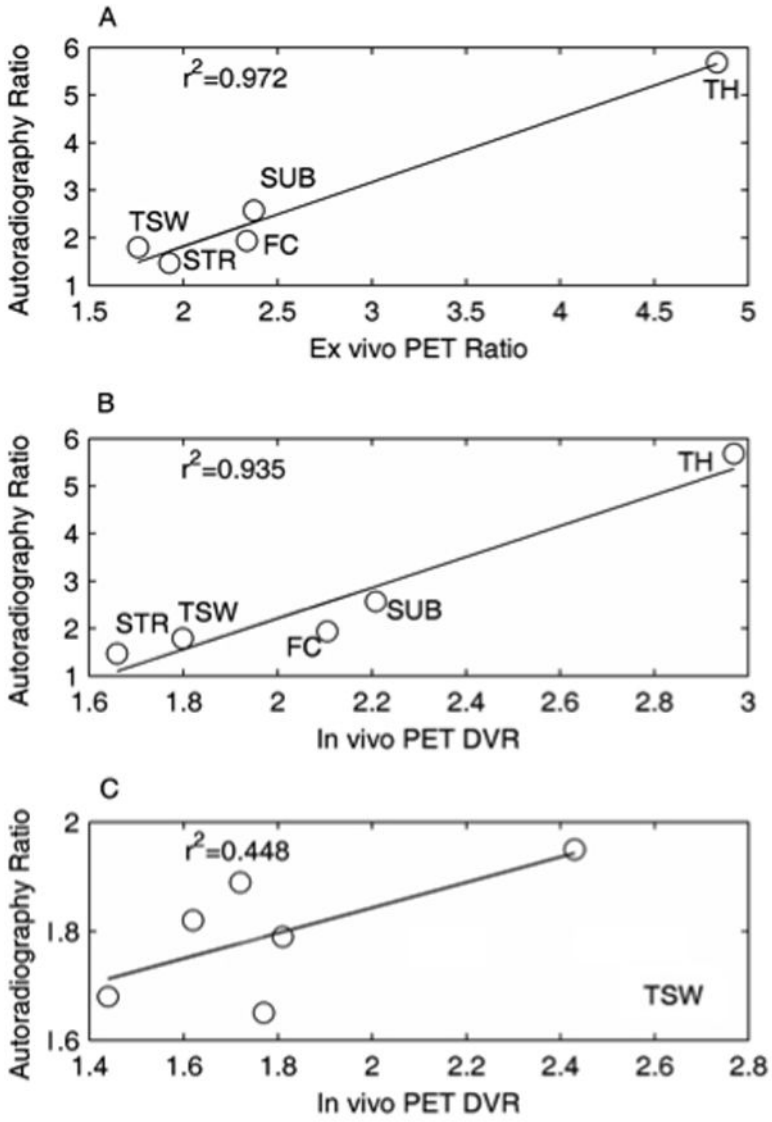

Figure 5.

Correlation of ^{18}F-nifene autoradiography to *ex vivo* PET (A) and *in vivo* PET (B) measures. Each data point represents an average of six animals, with CB in each animal used as a reference to normalize binding across animals. (C) Correlation of binding estimates from autoradiography vs. *in vivo* PET for TSW in six animals.

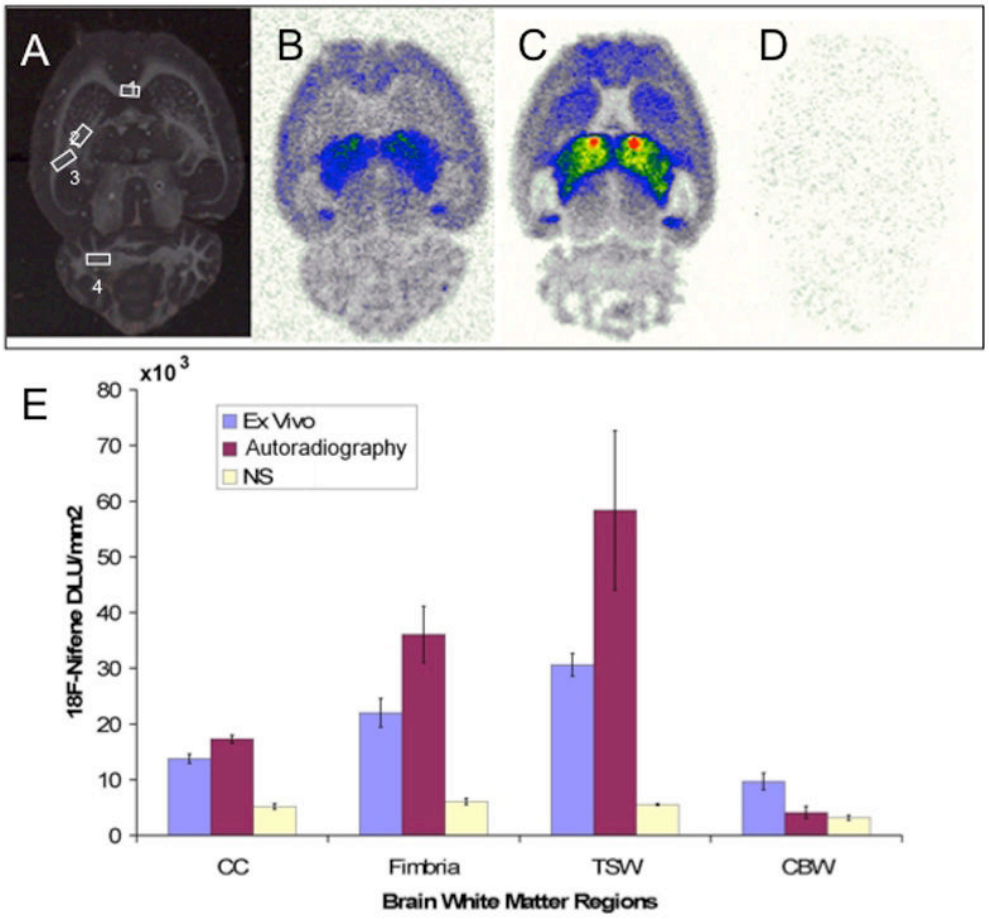

Figure 6.

^{18}F-Nifene binding in forebrain white matter. (A) Photoscan of a 40 μm tissue section showing regions of interest: corpus callosum (CC, 1), fimbria (2), TSW (3) and CB white matter (CBW, 4). (B) Same section as (A), showing ^{18}F-nifene autoradiography. (C, D). ^{18}F-nifene binding in the absence (C) and presence (D) of 300 mM nicotine to reveal nonspecific binding. (E) Mean ^{18}F-nifene binding in white matter for *ex vivo* PET and autoradiography (n = 4), and nonspecific (NS) binding (n = 2–3).

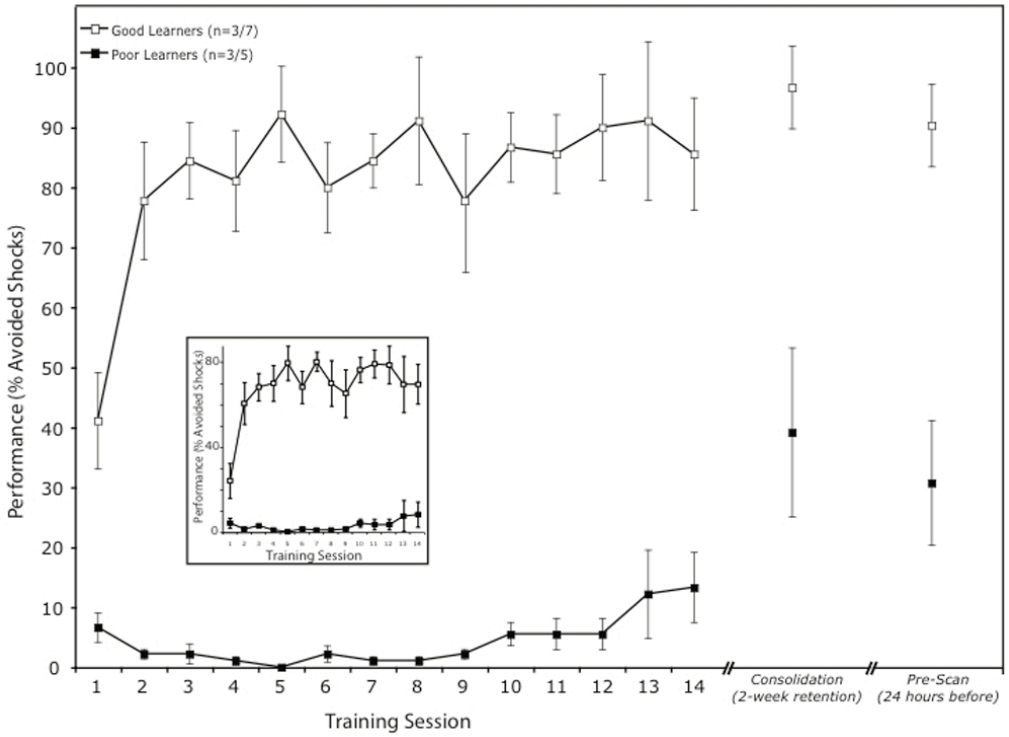

Figure 7.

Behavioral performance in an auditory-cued, active avoidance task over 14 days of training, followed by a retention test after two weeks, and a final test after variable delay before PET session. Performance is shown as mean (± sem) percentage of avoided shocks for the best- (n = 3) and worst- (n = 3) perfor ming animals; inset shows data for all 12 animals tested, separately for those that learned (n = 7) or did not (n = 5; see text for learning criterion).

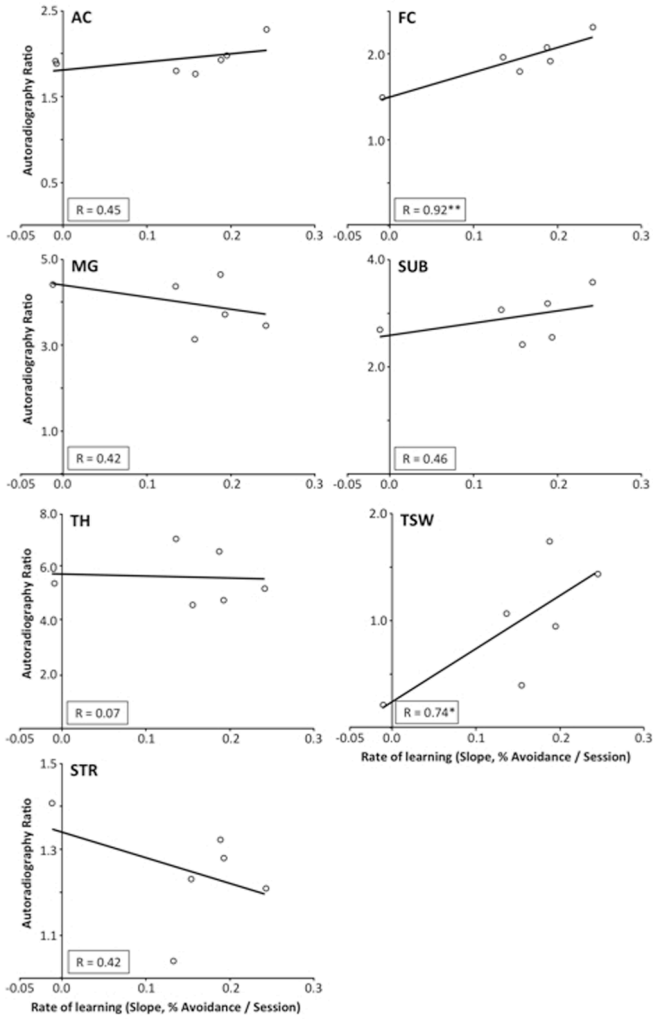

Figure 8.

Relation between ^{18}F-nifene binding in seven forebrain subregions and of initial learning rate for the three best- and three worst-performing animals. Autoradiographic binding was determined after all testing was completed, and was correlated with initial rate of learning (Table II, column 1), as an example of the analyses presented in Table II. Regression coefficient, R; *$p < 0.05$, or **$p < 0.01$).

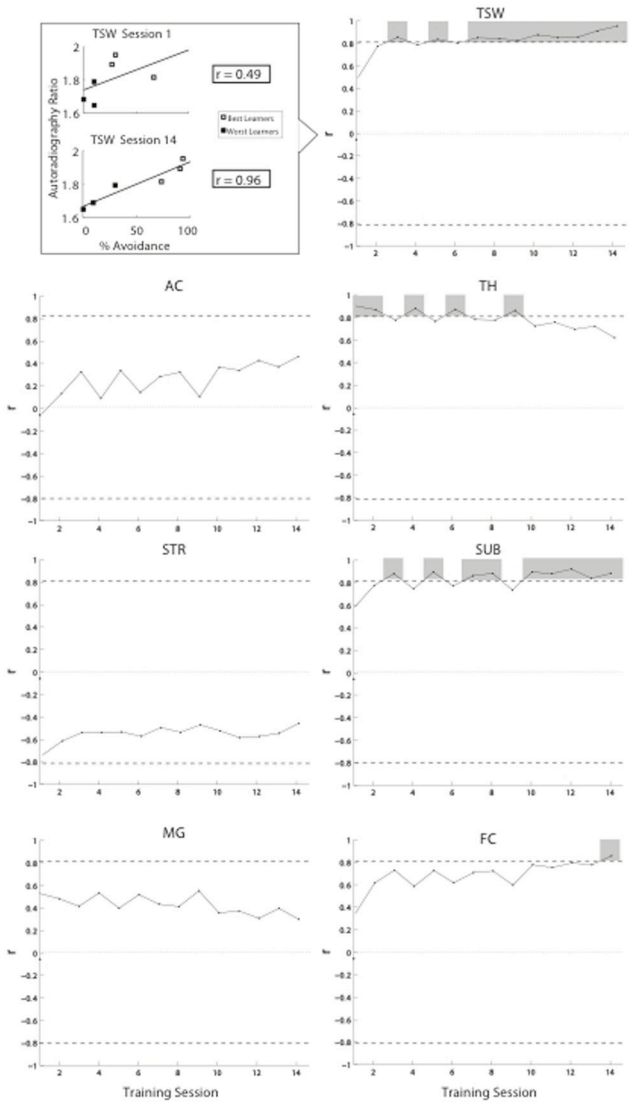

Figure 9.

Correlation of behavioral performance on each day of training with ^{18}F-nifene binding in forebrain subregions determined after all testing was completed. Data are for the 3 best- and 3 worst-performing animals (see top left for example, TSW binding vs. performance on training days 1 and 14; autoradiography ratio is binding relative to CB in the same animal). For each forebrain region, regression coefficients are plotted for each day; dashed line indicates threshold for significance ($p = 0.05$).

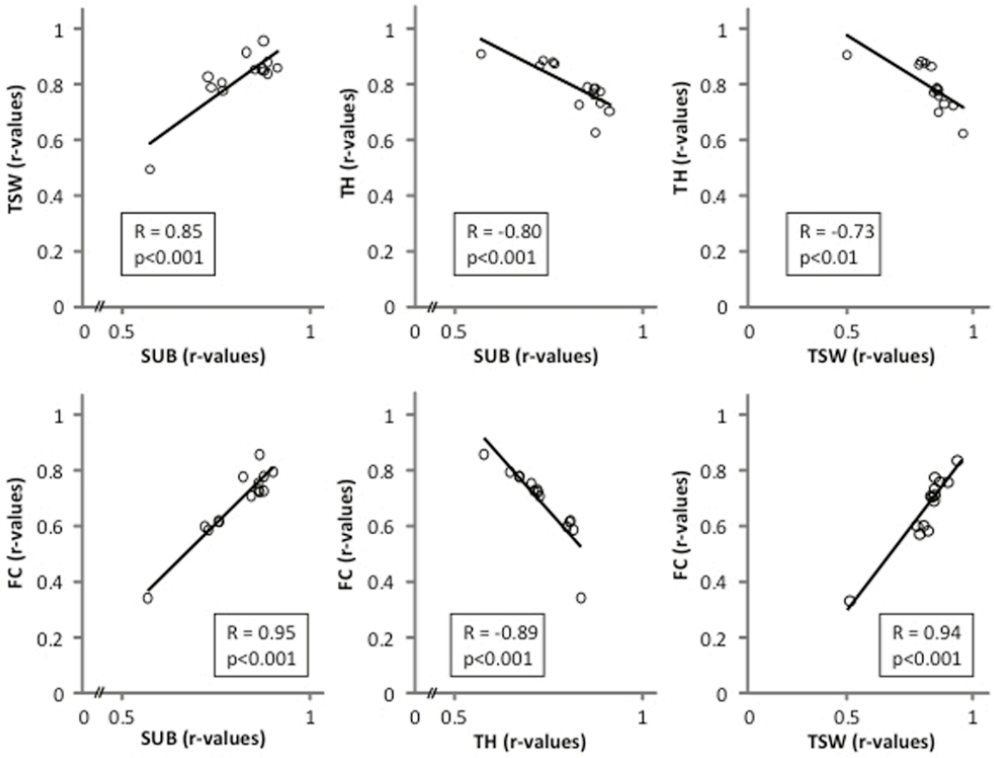

Figure 10.

Potential cooperativity among brain regions during learning. Regression data in Fig. 9 were correlated among pairs of brain regions, with significant correlations shown here. Negative correlations suggest a systematic transition from brain networks involving nicotinic regulation of TH to those involving TSW, FC and SUB.

Table I

Comparison of ^{18}F-nifene binding in rat forebrain regions using three imaging methods[1].

Brain region	*In vivo* PET[2]	*Ex vivo* PET[3]	Autoradiography[4]
TH	1.97 ± 0.66	4.84 ± 1.18	5.68 ± 1.00
SUB	1.21 ± 1.06	2.38 ± 0.29	2.58 ± 0.38
FC	1.11 ± 0.33	2.34 ± 0.38	1.94 ± 0.27
TSW	0.80 ± 0.34	1.76 ± 0.11	1.80 ± 0.12
STR	0.66 ± 0.33	1.93 ± 0.19	1.48 ± 0.06

[1] Mean (± SD) binding in six animals;

[2] BP_{ND} values calculated from *in vivo* PET studies using CB as reference;

[3] Ratios of brain regions vs. CB in summed *ex vivo* PET scans;

[4] Ratios for brain regions vs. CB in autoradiographic sections.

Table II

Correlation (r value) between behavioral performance and ^{18}F-nifene binding in rat forebrain regions[1]

	RATE OF AVOIDANCE LEARNING		LEVEL OF AVOIDANCE PERFORMANCE			MEAN AVOIDANCE LATENCY		FASTEST AVOIDANCE LATENCY	
Brain Region	**Learning Slope (%Avoidance/Session) (sess. 1–4)**	**First Trial # of 3 Consecutive "Avoided" Shocks**	**Asymptote (sess. 12–14)**	**Consolidation (sess. 15)**	**Retention (sess. 15–18)**	**Asymptote (sess. 12–14)**	**Retention (sess. 15–18)**	**Asymptote (sess. 12–14)**	**Retention (sess. 15–18)**
AC	0.45	0.29	0.41	0.16	0.23	0.16	0.08	0.33	0.23
MG	0.42	0.21	0.33	0.15	0.07	0.29	0.12	0.10	0.11
TH	0.07	−0.66	0.69	0.36	0.40	0.22	0.38	0.40	0.40
STR	0.42	0.64	−0.53	−0.70	−0.69	0.71	0.70	0.60	0.66
FC	0.92**	−0.84*	0.82*	0.87**	0.89**	−0.85*	−0.91*	−0.76*	0.89**
SUB	0.46	−0.81**	0.88**	0.53	0.59	0.42	−0.61	0.53	−0.63
TSW	0.74*	−0.89*	0.92**	0.79*	0.84*	−0.71	−0.83*	−0.79*	−0.82*

[1] Data from 6 animals;

* $p < 0.05$;

** $p < 0.01$.